

Fine-Grained Sports, Yoga, and Dance Postures Recognition: A Benchmark Analysis

Asish Bera, *Member, IEEE*, Mita Nasipuri, *Life Senior Member, IEEE*
Ondrej Krejcar, and Debotosh Bhattacharjee, *Senior Member, IEEE*

Abstract—Human body-pose estimation is a complex problem in computer vision. Recent research interests have been widened specifically on the Sports, Yoga, and Dance (SYD) postures for maintaining health conditions. The SYD pose categories are regarded as a fine-grained image classification task due to the complex movement of body parts. Deep Convolutional Neural Networks (CNNs) have attained significantly improved performance in solving various human body-pose estimation problems. Though decent progress has been achieved in yoga postures recognition using deep learning techniques, fine-grained sports, and dance recognition necessitates ample research attention. However, no benchmark public image dataset with sufficient inter-class and intra-class variations is available yet to address sports and dance postures classification. To solve this limitation, we have proposed two image datasets, one for 102 sport categories and another for 12 dance styles. Two public datasets, Yoga-82 which contains 82 classes and Yoga-107 represents 107 classes are collected for yoga postures. These four SYD datasets are experimented with the proposed deep model, SYD-Net, which integrates a patch-based attention (PbA) mechanism on top of standard backbone CNNs. The PbA module leverages the self-attention mechanism that learns contextual information from a set of uniform and multi-scale patches and emphasizes discriminative features to understand the semantic correlation among patches. Moreover, random erasing data augmentation is applied to improve performance. The proposed SYD-Net has achieved state-of-the-art accuracy on Yoga-82 using five base CNNs. SYD-Net’s accuracy on other datasets is remarkable, implying its efficiency. Our Sports-102 and Dance-12 datasets are publicly available at <https://sites.google.com/view/syd-net/home>.

Index Terms—Sports, Dance, Yoga, Attention, Convolutional Neural Networks (CNNs), Posture Recognition, Random Erasing.

I. INTRODUCTION

HUMAN body-pose recognition is a challenging problem in computer vision. It is widely used in various applications, such as sports [1]–[6], yoga [7]–[14], dance [15]–[19], daily activity [20], and others [14], [21], [22]. Among these actions and postures, Sports, Yoga, and Dance (SYD)

are intrinsically very important physical activities to balance functionalities of various body parts, well-being, etc. The SYD activities (Fig. 1) are crucial to improve our quality of life (QoL) and mitigating several diseases and mental health conditions, *e.g.*, Parkinson’s disease, anxiety, sleeping disorder, etc. [23]. Fine-grained image classification (FGIC) using SYD postures is difficult due to huge intra-class variations and small inter-class differences among the sub-categories. SYD express our emotion, complex body movements, gestures, costumes, and diversity. Dance is a perceptual domain integrating audio (music) and video (posture) in a synchronized manner to represent the underlying knowledge of a dance style [24]. In this direction, Indian Classical Dance (ICD) and Yoga poses (aka *asana*) effectively represent their heritage and culture since ancient times [25], [26]. Also, hundreds of dancing themes (*e.g.*, tribal, folk, etc.) are popular across the world. These diversities are promoted in the Intangible Cultural Heritage of UNESCO, such as the Lazgi (Khorazm region in Uzbekistan) [27], Thai (Thailand) Kolo (Serbia), Lad’s (Romania), Bharatnatyam (India), and others.



Fig. 1. Symbolic examples of fine-grained Sports, Yoga, and Dance (SYD) postures, represent complex body part movements and gestures, which are key challenges in posture recognition.

To address the challenges in SYD recognition, existing methods have emphasized hand-crafted features (*e.g.*, bag-of-words, haar wavelets, scale-invariant feature transform (SIFT), space-time interest points (STIP), moments, etc.) [28], [29], pose estimation from skeletal joints [22], [30], motion analysis using optical flow information [26], and deep convolutional features [18], [21], [31], shown in Table I. The pose estimation performance is remarkably improved using deep learning and related fusion-based techniques. Most of these methods are experimented with laboratory-simulated dance videos collected from YouTube, or other web resources, summarized in Table I. The Leeds Sports Pose (LSP) dataset [32] represents 8 sports classes. The Yoga-82 [8] comprised of 82 fine-grained yoga poses. Another dataset containing 107 yoga classes, Yoga-107, is also experimented. However, no image-based dataset with diverse variations of dance styles is publicly available. Our main motivation is to create new image-based dance and sports action datasets. We have presented the Sports image dataset with 102 actions, and the Dance image dataset with

A. Bera is with the Department of Computer Science and Information Systems, Birla Institute of Technology and Science, Pilani, Pilani Campus, Rajasthan, 333031, India. E-mail: (asish.bera@pilani.bits-pilani.ac.in).

M. Nasipuri is with the Department of Computer Science and Engineering, Jadavpur University, Kolkata 32, India. Email: mitanasipuri@gmail.com

O. Krejcar is with the Center for Basic and Applied Science, Faculty of Informatics and Management, University of Hradec Kralove, Rokitanskeho 62, 500 03 Hradec Kralove, Czech Republic. Email: ondrej.krejcar@uhk.cz

D. Bhattacharjee is with the Department of Computer Science and Engineering, Jadavpur University, Kolkata 32, India. He is also with the Center for Basic and Applied Science, Faculty of Informatics and Management, University of Hradec Kralove, Rokitanskeho 62, 500 03 Hradec Kralove, Czech Republic. Email: debotosh@ieee.org

TABLE I
SUMMARY OF A FEW EXISTING SPORTS, YOGA, AND DANCE RECOGNITION IMAGE/VIDEO DATASETS WITH RELATED DESCRIPTIONS.

| Ref, year | Method | Input data | Dataset name and pose/actions |
|------------|--|--|--|
| [32], 2010 | appearance and pose-based pictorial structure model. | 1000 training and 1000 testing images | Sports 8: Soccer, Tennis, etc. |
| [37], 2011 | global scene model with a figure-centric visual word representation | 150 clips (mean 6.39s) at 10fps | UCF Sports: kicking, lifting, riding horse, running, etc. |
| [38], 2014 | multiple schemes to learn spatio temporal features | 1 million YouTube videos, avg 5.36 min clip. | 487 classes: cricket, racing, etc. |
| [39], 2019 | spatio-temporal color-coded image called, joint angular displacement map (JADM). | 16,800 3D yoga videos with 400 videos per pose, collected using a mocap setup. | Yoga 42: standing postures, katchakrasana, etc. |
| [8], 2020 | classification using CNNs in a hierarchical structure | 28,478 yoga-pose images are collected from various search engines. | Yoga 82: Handstand, Plank, Side reclining, Shoulderstand, etc. |
| [7], 2022 | contrastive skeleton feature representations and extracts 33 keypoints using Mediapipe | contains 1931 images collected from Kaggle | Yoga 45: balancing, sitting, upward bow pose, etc. |
| [40], 2013 | space-time interest point descriptors computed from each frame and classified by a non-linear SVM. | 330 video clips of 87 dancers at 30 fps, and collected from stage performance. | ICD - 6 styles: Bharatanatyam, Kathak, Odissi, etc. |
| [41], 2017 | mid-level action representation using dancelets for dance-based video recommendation. | 420 videos collected from YouTube and Youku websites. | HIT Dances 6 styles: Ballet, Hip-hop and 4 Chinese folks. |
| [42], 2018 | integrates optical flow and motion data. Fusion-based multi-stream 3D temporal CNNs were tested. | 1000 videos of 10 sec. at 30 fps, a total of 300000 frames. | Let's Dance 10 classes: Ballet, Foxtrot, Latin, Tango, etc. |
| [43], 2021 | Estimates 2D pose sequences, and tracks dancers. Simultaneously estimates corresponding 3D poses. | 1143 video clips of 9 genres, 154 movement types of 16 body parts. | University of Illinois Dance - 9 types: Ballet, Tango, etc. |
| [44], 2022 | understanding dance semantics by spatio temporal dynamics using keypoints (OpenPose) and GRU. | 300 HD dance videos, collected from 6 performers in indoor and outdoor, and YouTube. | 7 types: firing arrows, dance of peacock, playing flute, etc. |
| Ours, 2023 | Multi-scale patch-based attention mechanism | 5967 image samples collected from Kaggle | Yoga 107: tulasana, lolasana, etc. |

12 categories, which are the first of their kind. A new deep model is devised to simulate experimental analysis on four SYD datasets in a weakly supervised manner.

We have proposed a patch-based attention (PbA) module, namely SYD-Net (Fig. 2), that integrates spatial attention and channel attention on top of standard backbone convolutional neural networks (CNNs). Our aim is to establish a semantic correlation among a set of uniform and multi-scale patches by focusing on the most relevant image regions for defining a comprehensive feature descriptor. SYD-Net is inspired by the self-attention mechanism [33], [34], which is an integral ingredient of numerous deep architectures in computer vision and natural language processing ubiquitously. Gaussian dropout [35] is adapted to hinder overfitting. Random region erasing [36] data augmentation (Fig. 3) produces on-the-fly data diversity for effective training of SYD-Net. The major contributions of this work are:

- A patch-based attention mechanism that summarizes the discriminativeness of partial feature descriptors for fine-grained sports, yoga, and dance postures recognition.
- A new image dataset with 102 sport actions and another dataset representing 12 dance styles are proposed for posture classification avoiding part-based/skeletal-joint/bounding-box information.
- Extensive experiments are conducted using five backbone CNN architectures on four SYD datasets in a weakly supervised manner.
- The proposed SYD-Net approach achieves state-of-the-art accuracy on the Yoga-82 and Yoga-107 datasets.

The rest of this paper is organized as follows: Section II summarizes related works on SYD poses. Section III describes the proposed method. Section IV describes the datasets briefly. Section V demonstrates the experimental results of the ablation study. The conclusion is presented in Section VI.

II. RELATED WORKS

Posture recognition methods can be generalized into two broader streams: a) hand-crafted, and b) deep-learning methods including, attention-based works. Some SYD pose recognition methods are summarized in Table I, and described next.

A. Study on Sports Actions

Sports activities are primarily recognized using deep architectures. Various sports technologies and related datasets are studied and analyzed the role of computer vision technologies in sports (*e.g.*, player and ball tracking) in [5]. The pictorial structure model (PSM) with clusters of partial pose descriptors from sports images is presented [45]. The dataset is more challenging than its earlier version, called Leeds Sports Pose (LSP) dataset [32]. The collective sports video dataset represents a multi-task recognition of both 5 collective activities and 11 sports categories [6]. Deep learning methods using CNNs and long short-term memory (LSTM) are tested for benchmark analysis. A two-stream attention model using LSTM is described for action recognition [4]. Freestyle wrestling actions are recognized from videos using a histogram of graph nodes [46]. A multi-labels DeepSport dataset is presented for automated sport understanding using videos captured at multiple views of a basketball game [1]. A CNN combining global regression and local information refinement modules for sports-pose estimation using 2D images is presented [3]. Swimming motion analysis is presented [14]. Figure Skating Dataset with 10 sports actions (FSD-10) is introduced for fine-grained content analysis using a key-frame-based temporal segment network [47]. Most of the existing works on sports analysis are based on video datasets.

B. Study on Yoga Postures

Mainly, three types of intelligent approaches for yoga pose analysis have been developed: (a) wearable device, (b) Kinect, and (c) computer vision. A hybrid multi-modal and body multi-positional system for recognizing 21 complex

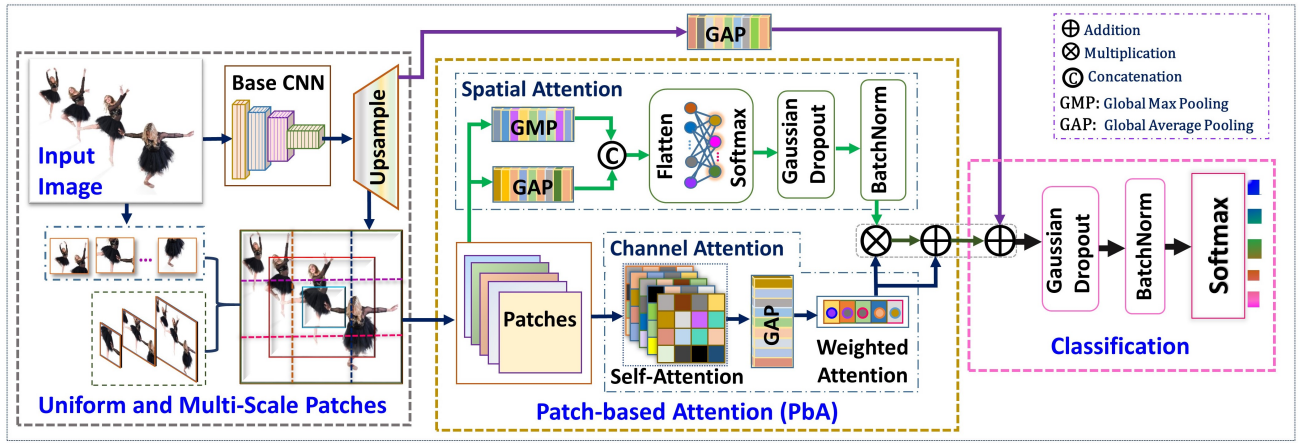


Fig. 2. Proposed SYD-Net Model comprises three key modules. a) Extraction of hybrid patches, consisting of same-size uniform patches and hierarchical multi-scale regions. b) Patch-based attention module, consisting of the self-attention feature maps and further refined with the weighted-attention to define channel-attention. It is modulated with a spatial attention module to define an attentional feature map. c) Finally, the compact feature vector is regularized with the Gaussian dropout and batch normalization prior to the softmax layer for classification.

human activities using wearable devices is developed [48]. The CNNs recognize yoga poses from 3D motion capture data by integrating a joint angular displacement map (JADM) comprising 39 joints of yoga action skeletons [39]. A yoga pose grading approach is described using contrastive skeleton feature representations [7]. Many approaches have used OpenPose to estimate the keypoints/joints in developing Yoga pose recognition and mobile applications for self-assessment and yoga assistance [49]–[51]. A yoga self-coaching system using an interactive display in real time is developed to avoid incorrect postures [52]. It classifies 14 yoga postures based on transfer learning. The fitness actions of 28 poses are classified into three categories of exercises [10]. Likewise, 88 videos are used for classifying 6 Yoga poses [49]. Yoga-82 [8] has introduced a new dataset containing almost 28.5k images of 82 fine-grained yoga poses, and illustrated in Fig. 7. This dataset is tested in our study for further improvement.

C. Study on Dance Postures

Traditional hand-crafted feature-based and deep learning approaches are developed for dance posture recognition. The bag-of-words method is applied to recognize five Greek dance styles from videos [53]. The space-time interest point (STIP) detection and their description from videos using a 3D facet model are presented [54]. A spatio temporal Laban feature descriptor (STLF) from YouTube videos is described [55]. Using a Kinect sensor, 3D skeletal information of 25 leg postures from five dancers representing *Odisi* dance has been collected, and a similarity function is used for recognition [30]. Multiple kernel learning using a directed acyclic graph is presented [29]. With music, *Kathakali* demonstrates complex hand gestures, body movements, and facial expressions. The dataset contains 654 images representing 24 mudras of *Kathakali* and was tested using CNN [56]. *Bharatanatyam* posture recognition is tested on audio and video data using the Gaussian mixture model (GMM), support vector machine (SVM), and CNN [57]. Dance semantics understanding from videos by deep pose estimation (based on OpenPose) coupled with a gated recurrent unit (GRU) is presented [44]. The

Inception-v3 features, 3D CNN features, and pose signature based on AlphaPose estimation are combined and fed into an LSTM for building spatio temporal relationships for ICD classification [58]. A model based on ResNet-50 recognized eight ICD [59]. An Uzbek national dance, *Lazgi* classification and recognition using an optical motion capture system are explored [27]. According to our study, image datasets representing various sport actions and dance styles are unavailable for weakly supervised pose estimation. This work presents two new image datasets for sport and dance actions recognition.

III. PROPOSED METHOD

Sports, Yoga, and Dance (SYD) involves complex movements of body parts and subtle variations in expression and gesture, *e.g.*, yoga and dance poses. Human-object interactions could also be involved, *e.g.*, players with a football in sports. Various pose-estimators, object detectors, skeletal joints, and body parts are often used to solve the problem. The recognition task becomes more challenging when multiple persons are involved in an activity. In some cases, extraction and localization of body keypoints of multiple persons from a still image could be burdensome, and difficult to formulate an appearance-based model. Sometimes, a global descriptor overlooks finer details, which are essential for FGIC [60]. Our intuitive approach is that region-based partial feature description could be an alternative solution in capturing finer details of SYD poses for classification. Our target is to devise an end-to-end trainable deep architecture to classify these complex fine-grained human postures avoiding any bounding-box annotation, object/pose detector, and body keypoints/joints, commonly used in existing works. Moreover, the random erasing technique with conventional data augmentation is followed for additional benefits to ease overfitting and overall performance gain. The proposed SYD-Net, conceptualized in Fig. 2, is divided into three parts: a) computing a set of non-overlapped patches with fixed-size and multi-scale region proposals, b) patch-based attention module, and c) classification. Functionalities of all modules are described next.

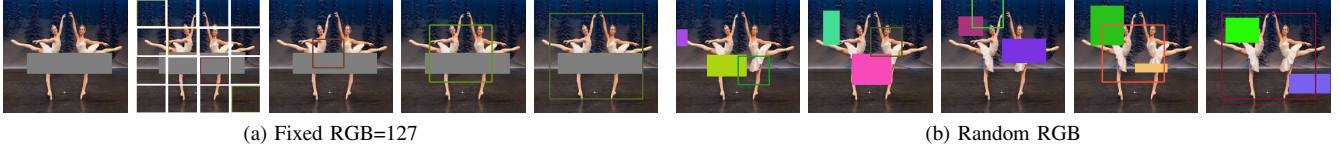


Fig. 3. Patches with random erasing image augmentation. (a) Erased full image with fixed RGB=127; 4×4 uniform, and multi-scale patches, enclosed by rectangles. (b) Two random regions erased with random RGB colors on both types of patches.

A. Uniform and Multi-Scale Patch Proposals

In an image, contextual information and associated object(s) provide a vital cue to understand human activity, evident in various sports (Fig. 5). Here, a patch-based approach is devised to learn overall semantics and contexts from various image parts at multiple scales (Fig. 3). We aim to integrate detailed information from several smaller non-overlapping image patches into a comprehensive feature descriptor. Moreover, hierarchical regions establish a semantic correlation and contextual representation among the feature maps. The uniform patches focus on finer details in each small region. Whereas larger multi-scale patches summarize overall feature representation holistically. Thus, combining these two key aspects through an attention mechanism improves overall efficiency for subtle discrimination in fine-grained SYD postures.

Let a color input image $I_l \in \mathbb{R}^{h \times w \times 3}$ is fed into a backbone CNN, such as MobileNet-v2 with class-label l . A backbone network \mathcal{N} extracts high-level feature maps $\mathbf{F} \in \mathbb{R}^{h \times w \times c}$ where h , w , and c denote the height, width, and channels, respectively. The input image I_l is divided into a set (D) of non-overlapping uniform patch proposals. The resulting number of small regions is $e = (h \times w)/a^2$, where $a \times a$ is the spatial size of a rectangular patch d . Set $D = \{d_1, d_2, \dots, d_e | I_l\}$ consists of e parts. A small patch d_i is defined with its spatial dimension $p_i = [x_i, y_i, \Delta w, \Delta h]$, and here $\Delta w = \Delta h = a$ is uniformly the same for all patches. Each patch is denoted as $d_i = [\mathbf{F}_i, p_i]$, where \mathbf{F}_i is the feature map of patch p_i . In addition, multi-scale patches are defined to capture complementary information hierarchically, where the patch sizes are progressively increasing. It can be defined as $p_i = [x_i, y_i, \Delta w_i, \Delta h_i]$ and $p_j = [x_j, y_j, \Delta w_j, \Delta h_j]$ such that $\Delta w_i > \Delta w_j$ and $\Delta h_i > \Delta h_j$, where $p_i > p_j$ regarding the spatial dimension of p_i and p_j patches, respectively. Finally, a collection of all n patches (*i.e.*, uniform and multi-scale) is denoted as $P = \{p_i\}_{i=1}^{i=n}$, and corresponding feature map is $\mathbf{F} = \{\mathbf{F}_i\}_{i=1}^{i=n} \in \mathbb{R}^{n \times (h \times w \times c)}$. The feature map of each patch is determined through a mapping between the correspondence of smaller regions within the actual high-level output feature maps, extracted using a base network \mathcal{N} . Firstly, \mathbf{F} is upsampled to a higher resolution $k(h \times w)$ for this intent. Then, bilinear interpolation is applied for pooling features from every patch. The upsampling is regarded as a mapping $m : \mathbf{F} \rightarrow \mathbf{F} \in \mathbb{R}^{k(h \times w) \times c}$, where actual spatial size ($h \times w$) is scaled up by k times before pooling. Though P represents patches of various sizes, bilinear pooling renders the feature vectors of the same sizes for all patches, which are kept the same as the output dimension of base CNNs, *i.e.*, $\mathbf{F} \in \mathbb{R}^{(h \times w \times c)}$, and denoted as \mathbf{F} .

B. Patch-based Attention (PbA) mechanism

Attentional feature description is proliferated ubiquitously in image recognition and others to improve performance. Here, attention is performed in two paths, patch-based channel attention and spatial attention, which are finally integrated together. It fuses both to summarize essential features by exploring *where* to focus and *what* to emphasize simultaneously in the feature maps \mathbf{F} . Self-attention acts across the channel-based feature maps of all patches to capture channel-wise relationships. It relates inter-channel feature interactions among patches and estimates their relevance correspondingly. Cross-channel attention investigates the importance of feature maps (*what*) to enhance learning capability. On the contrary, spatial attention explores neighborhood structural interpretation for producing a spatial attentional mask (*where*) for further refinement of aggregated feature summarization. These dual-attention pathways empower significantly and act complementarily to render a global information for distinguishing subtle variations in SYD recognition.

1) *Channel Attention (CA)*: Channel attention is adapted from self-attention mechanism that tackles long-range dependency by generating a context vector based on the weighted sum of feature space [33], [34]. In self-attention, the query \mathbf{Q} , key \mathbf{K} , and value \mathbf{V} are learned from the same input feature vector \mathbf{F} . The attention-weight matrix is a dot product of \mathbf{Q} and \mathbf{K} , multiplied by \mathbf{V} to generate an attention-focused feature map. We have applied $[Q, K, V]$ attention principle for a patch p_i and its neighbors p_j patches ($i \neq j$). We aim to generate an attentional feature descriptor, *i.e.*, value \mathbf{V} that focuses on the relevant and discriminative regions. \mathbf{F}_i and \mathbf{F}_j are high-level feature vectors computed from p_i and p_j patches, respectively. The attentional feature map is given as

$$\begin{aligned} \psi_{i,j} &= \tanh(\mathbf{W}_\psi \mathbf{F}_i + \mathbf{W}_{\psi'} \mathbf{F}_j + \mathbf{b}_\psi), \\ \vartheta_{i,j} &= \sigma(\mathbf{W}_\vartheta \psi_{i,j} + \mathbf{b}_\vartheta) \end{aligned} \quad (1)$$

where \mathbf{W}_ψ and $\mathbf{W}_{\psi'}$ are the weight matrices to compute attention vectors using p_i and p_j patches, respectively; \mathbf{W}_ϑ is their nonlinear combination; \mathbf{b}_ψ and \mathbf{b}_ϑ are the bias vectors, and $\sigma(\cdot)$ is element-wise nonlinear activation. The next objective is to compute the importance of each p_i through a weighted sum of attention scores of all patches, given as

$$\delta_{i,j} = \text{softmax}(\mathbf{W}_\delta \vartheta_{i,j} + \mathbf{b}_\delta), \hat{\mathbf{F}}_i = \sum_{j=1}^n \delta_{i,j} \mathbf{F}_j \quad (2)$$

where \mathbf{W}_δ is the weight matrix, and \mathbf{b}_δ is the bias vector. The aggregated feature space is $\hat{\mathbf{F}}_i$ which is summarized through a global average pooling (GAP) layer to generate $\tilde{\mathbf{F}}_i$ for all patches in P . The result $\tilde{\mathbf{F}}_i$ is passed through a *softmax* layer for producing a weighted attention matrix ϕ_i . Finally, their

weighted sum \mathbf{F}_{CA} is considered as the output of the cross-channel attention (CA) mechanism, and is given as

$$\tilde{\mathbf{F}}_i = \mathcal{GAP}(\hat{\mathbf{F}}_i), \mathbf{F}_{CA} = \sum_{i=1}^n \phi_i \tilde{\mathbf{F}}_i \quad (3)$$

where, $\phi_i = \text{softmax}(\mathbf{W}_\phi \tilde{\mathbf{F}}_i + \mathbf{b}_\phi)$

2) *Spatial Attention (SA)*: Spatial attention captures the neighborhood information to calibrate feature representation by generating an attentional mask for refining the global structural information. This mask builds spatial relationships by correlating *where to pay attention* in the feature space. Thus, it effectively localizes the most informative region(s) for global semantic representation of SYD postures.

No parameter optimization is required in the global average pooling (GAP), and it helps to avoid overfitting [61]. GAP sums out spatial information; thus, it is more robust to spatial translations of input. It can play as a structural regularizer in the network. Here, GAP is applied to refine spatial features \mathbf{F} from all patches P . It downsamples the channel dimension precisely to $(h \times w \times 1)$ by summarizing the mean features and generating \mathbf{F}_{gap} . Compared to GAP (\cdot), global max pooling (GMP) emphasizes the most important features from cross-channels and generates an optimized feature vector \mathbf{F}_{gmp} . A combination of both pooling improves learning efficiency compared to any single pooling [62]. The fused feature map $\mathbf{H} \in \mathbb{R}^{n(h \times w \times 2)}$ is defined as

$$\mathbf{H} = \text{concat}(\mathcal{GAP}(\mathbf{F}); \mathcal{GMP}(\mathbf{F})) \quad (4)$$

where, the feature pooling is $\mathbf{F} \rightarrow \mathbf{F}_{gap} : \mathbb{R}^{n(h \times w \times 1)}$, and same for \mathbf{F}_{gmp} . Next, a multi-layer perceptron (MLP) is applied to generate a spatial attention mask \mathbf{F}_{SA} . A MLP layer comprises a flatten, softmax, Gaussian dropout, and batch normalization layers. We aim to compute weighting factors based on the probabilities rendered by softmax activation. The probabilities are computed by a dense layer with the same size as base CNNs output channels $1 \times c$.

$$\mathbf{F}_{SA} = \mathcal{MLP}(\mathbf{H}); (\text{softmax} + \lambda_{GD+BN}) \Rightarrow \mathcal{MLP} \quad (5)$$

where λ_{GD+BN} denotes a regularization (λ) process with a Gaussian dropout (GD) and batch normalization (BN) layers. The spatial attention mask is $\mathbf{F}_{SA} \in \mathbb{R}^{(1 \times c)}$. This patch-level spatial attention (\mathbf{F}_{SA}) mask is multiplied element-wise with the weighted attention vector \mathbf{F}_{CA} , rendered from channel attention method. It modulates overall feature representation and empowers discriminability by capturing subtle details with focusing on global structural information, as essential for FGIC. A residual path is connected with \mathbf{F}_{CA} for smoother gradient flow in learning. Finally, a patch-based attention (PbA) feature vector $\mathbf{F}_{PbA} \in \mathbb{R}^{(1 \times c)}$ is obtained.

$$\mathbf{F}_{PbA} = (\mathbf{F}_{CA} \otimes \mathbf{F}_{SA} + \mathbf{F}_{CA}) \quad (6)$$

3) *Classification*: The upsampled feature \mathbf{F} is squeezed by a GAP layer to produce a vector of $(1 \times c)$ channels which is added with attentional feature map \mathbf{F}_{PbA} . The final feature

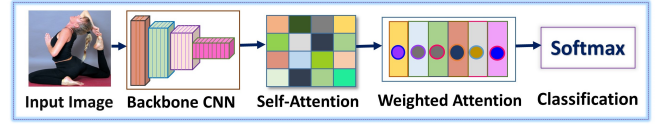


Fig. 4. Baseline approach using attention over CNN's output features.

vector \mathbf{F}_f is regularized and passed to a softmax layer to compute an output vector implying the class probabilities.

$$\mathbf{F}_f = \mathbf{F}_{PbA} + \mathcal{GAP}(\mathbf{F}); Y_{pred} = \text{softmax}(\lambda(\mathbf{F}_f)) \quad (7)$$

Gaussian dropout (GD) [35] and batch normalization (BN) regularizers are applied to avoid overfitting issues and denoted as λ . The GD can generalize learning tasks effectively than a simple dropout layer. Typically, GD uses multiplicative noise, and the dropout rate ϕ maps to the noise standard deviation σ_{noise} . This hyperparameter is computed as $\sigma_{noise}(\rho) = \sqrt{\rho \cdot (1 - \rho)^{-1}}$. The noise distribution is free of learnable parameter. The categorical cross-entropy loss function $\mathcal{L}_{ce}(Y_{true}, Y_{pred})$ minimizes the error rates between the actual class-label (Y_{true}) and predicted class-label (Y_{pred}) during the learning task. The proposed SYD-Net is end-to-end trainable and the attention module could be added with standard backbones to enhance efficiency.

C. Attention-based Baseline Method

In addition to the conventional baseline evaluation, the attention mechanism is applied to compute baseline results (Table III). We aim to observe the suitability of hybrid patches in improving the accuracy of attention-based baseline results using different backbone CNNs. A pictorial representation of the attention-based baseline is shown in Fig. 4. In this method, firstly, the high-level feature map from a backbone CNN is extracted. Subsequently, the self-attention and weighted attention techniques are exploited for re-weighting the base CNN's output features. Lastly, a softmax layer is applied to the attentional feature description for classification.

In summary, three methods are explored for baseline assessment: (a) simple classification method using high-level feature vector of a base CNN with conventional data augmentation; (b) similar classification strategy as (a), with additional random erasing data augmentation for more data-diversity; and (c) leveraging attentional weights over base CNN's features in conjunction with (b), shown in Fig. 4. Description of baseline evaluations is given in Sec. V-B. Indeed, our attention-based baseline performance outperforms the traditional baseline method that only uses base CNN's output features.

IV. DATASET DESCRIPTION

We have described the Sports-102, Yoga-82, Yoga-107, and Dance-12 datasets which provide only class labels, avoiding bounding-box annotations, and summarized in Table II.

1) *Sports-102 Dataset*: The sports dataset represents 102 sports-action classes representing complex human body postures. Sports-102 comprises various games, some of which are based on individual performers (e.g., golf, javelin, etc.) while others are team-based (e.g., hockey, kabaddi, etc.) with diversity. Samples of various sports are shown in Fig. 5. The



Fig. 5. Examples of diverse sport actions from the Sports-102 dataset.

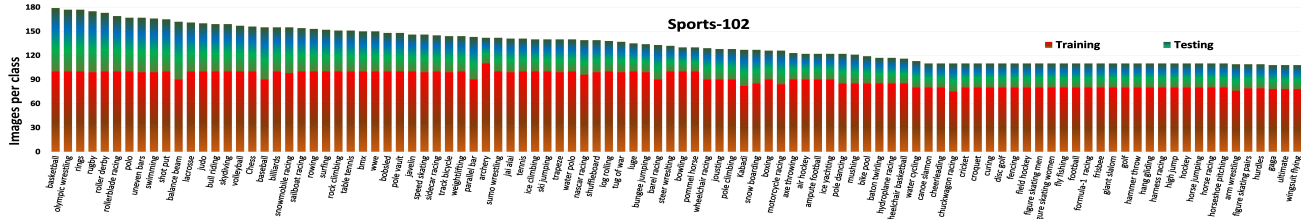
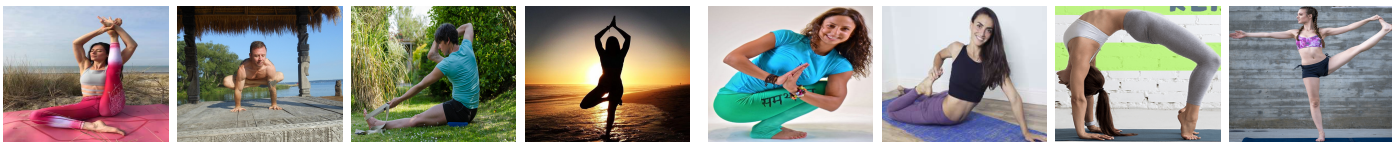


Fig. 6. Class-wise train-test image distribution of Sports-102 dataset. Best view of the class labels in zoom.



(a) Yoga-82 dataset

(b) Yoga-107 dataset

Fig. 7. Examples of various asanas from the Yoga-82 [8] and Yoga-107 datasets.

training and testing data distribution of various sports categories are shown in Fig. 6. Mainly, the images are collected from Kaggle¹ repository, and related websites. Though few video-based datasets exist for dance and sport actions, no such image-based datasets are publicly available for research, to the best of our knowledge.

2) *Yoga-82 [8] and Yoga-107 Datasets*: These are publicly available datasets. Samples of various postures of Yoga-82 are illustrated in Fig. 7.a. After careful observation, a few samples are rejected, which are irrelevant. The reason might be the resolution, format, size, other characteristics of images, and repetition of the same images. Some poses (*asana*) representing the cartoon’s and animal’s images are irrelevant to the current problem, so, eliminated. Thus, samples from various yoga classes are discarded to formulate a well-defined and precise Yoga-82 sub-dataset. Actual Yoga-82 contains 21.0k training and 7.4k testing samples. Whereas we have tested on 19.9k training and 7.2k testing images after standardization.

The Yoga-107 dataset is collected from Kaggle² repository and a few samples are shown in Fig. 7.b. It contains 107 fine-grained classes of yoga poses, comprising a total of 5.9k images. It is a challenging yoga dataset as the classes are more than 100, and the *asana* samples per class are much lesser than Yoga-82.

3) *Dance-12 Dataset*: A total of 12 dance styles are incorporated in the Dance-12 dataset representing diverse variations in postures, number of persons, background, theme, and other factors. This dataset represents the following

TABLE II
DATASET SUMMARY AND TOP-1 ACCURACY (%) OF SYD-NET TRAINED FROM SCRATCH AND WITH IMAGENET WEIGHTS USING XCEPTION.

| Dataset | Train | Test | Class | Xcep (srth) | Xcep (ImNet) |
|------------|-------|------|-------|-------------|--------------|
| Sports-102 | 9278 | 4315 | 102 | 96.70 | 98.86 |
| Yoga-82 | 19941 | 7241 | 82 | 97.29 | 97.80 |
| Yoga-107 | 4084 | 1883 | 107 | 82.00 | 85.20 |
| Dance-12 | 3129 | 1694 | 12 | 92.24 | 97.98 |

dance categories: Ballet, Hip-hop, Pole, Salsa, Samba, Bharatnatyam, Chau, Dandya, Dhunuchi, Kathak, Kalbelia, and Manipuri. The first five dances are internationally popular and the remaining seven are Indian. All the images are collected freely from various public websites such as Google, Yahoo, Bing, etc. Samples of international and Indian dance genres are illustrated in Fig. 8. The training and testing splits of various dance styles are given in Fig. 9. The purpose of our data collection is research only. No commercial gain or unethical issue is involved in our research. Dance-12 is growing a dataset in size and variations. We will include several more classical and folk dance styles from various countries around the world in the near future. This dataset is publicly available at <https://sites.google.com/view/syd-net/home>.

V. EXPERIMENTAL RESULTS

Firstly, we have analyzed the experimental details of SYD-Net. Next, an ablation study is presented to evaluate the significance of key components of the SYD-Net model.

A. Implementation

Our model is implemented using ResNet-50 [63], DenseNet-201 [64], NASNetMobile [65], MobileNet-v2 [66], and Xcep-

¹www.kaggle.com/datasets/gpiosenka/sports-classification

²<https://www.kaggle.com/datasets/shrutisaxena/yoga-pose-image-classification-dataset>

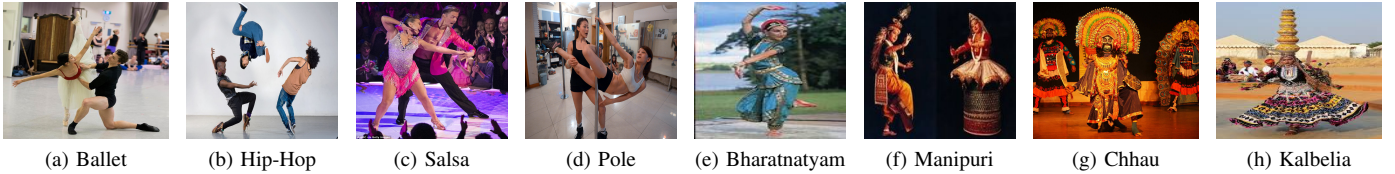


Fig. 8. Examples of various dance styles from the Dance-12 dataset.

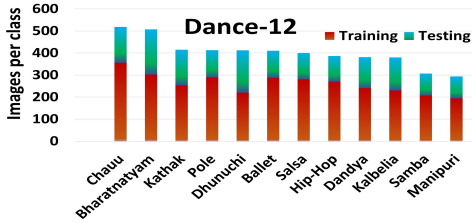


Fig. 9. Training-testing image distribution of Dance-12 dataset.

tion [67] backbone CNNs in TensorFlow-2.x with cuDNN 7.6. The input image resolution is 224×224 , and the output feature map of the MobileNet-v2 backbone is $7 \times 7 \times 1280$. Whereas, the output feature maps of other backbones represent the same spatial size, but differ in channel dimensions. The patch sets are extracted along the spatial dimension [68]. The spatial size of base output (7×7) is upsampled to 48×48 for extracting the patch sets from P_9 to P_{20} . The upsampled resolution is 45×45 for proper pixel alignment with the patch-sizes of P_{25} and P_{30} . Three sets of uniform patches (3×3 , 4×4 , and 5×5) and corresponding hierarchical regions are generated. For example, with 16 uniform patches, 4 multi-scale patches are computed in a hierarchical manner from the center of the input image with the smallest 12×12 size, and incremented to 24×24 , 36×36 , and finally to 48×48 size. Altogether 16 uniform and 4 hierarchical patches are considered in set P_{20} . Likewise, P_{12} and P_{30} are generated. Initially, the input image size is 256×256 . We have applied standard data augmentations of random rotation (± 25 degrees) and random scaling (1 ± 0.25). Two randomly selected regions of total size or a single region with size (0.1-0.8) are erased with either a fixed RGB=127 or random RGB pixel-values at a time (Fig. 3), and applied on-the-fly for image augmentation. Then, random cropping is applied to select an image size of 224×224 as input to CNNs. SYD-Net is trained from scratch for initializing base CNNs for a fair comparison, as well as trained with ImageNet weights in separate experiments. The Stochastic Gradient Descent (SGD) is used to optimize the categorical cross-entropy loss function with an initial learning rate of 0.007 and multiplied by 0.1 after every 50 epochs. The model is trained for 200 epochs with a mini-batch size of 8 using a Tesla M10 GPU of 8 GB. A Gaussian dropout rate 0.2 and batch normalization are applied to avoid overfitting. The top-1 and top-5 accuracy (%) metrics are used for performance evaluation, and the model’s parametric complexity is estimated in millions (M).

TABLE III
TOP-1 BASELINE ACCURACY (%) USING CONVENTIONAL DATA AUGMENT (TOP ROW-SET), RANDOM ERASING AUGMENT (MID ROW-SET), AND ATTENTION WITH RANDOM ERASING (LAST ROW-SET). THE LAST COLUMN SHOWS MODEL PARAMETERS IN MILLIONS (M).

| Base CNNs | Sports | Yoga-82 | Yoga-107 | Dance | Par (M) |
|--------------|--------------|--------------|--------------|--------------|---------|
| ResNet-50 | 68.34 | 75.52 | 52.13 | 63.44 | 23.8 |
| DenseNet-201 | 74.21 | 80.16 | 55.12 | 68.12 | 18.5 |
| MobileNet-v2 | 75.70 | 79.73 | 60.31 | 63.80 | 2.4 |
| Xception | 79.10 | 81.93 | 62.87 | 72.27 | 21.1 |
| ResNet-50 | 70.91 | 77.56 | 55.28 | 63.80 | 23.8 |
| DenseNet-201 | 76.69 | 80.60 | 57.47 | 68.24 | 18.5 |
| MobileNet-v2 | 77.62 | 82.23 | 65.10 | 65.58 | 2.4 |
| Xception | 80.17 | 83.78 | 66.50 | 72.92 | 21.1 |
| ResNet-50 | 70.96 | 80.60 | 57.31 | 60.90 | 23.9 |
| DenseNet-201 | 77.18 | 83.63 | 58.38 | 68.95 | 18.6 |
| MobileNet-v2 | 77.22 | 83.31 | 65.86 | 68.06 | 2.4 |
| Xception | 82.88 | 85.67 | 67.52 | 73.34 | 21.2 |

B. Performance Analysis

The performances of SYD-Net have been evaluated considering several important aspects, discussed next.

1) *Baseline Results*: First, baseline performances of four backbone CNNs (trained from scratch) are computed on four datasets. The results are given in Table III. Three sets of experiments are conducted for a baseline evaluation, as aforesaid. In the first set of experiments (top row set), conventional data augmentations, *i.e.*, rotation, scaling, and cropping are applied. In addition to the general augmentation, random region erasing is applied in the second set of experiments, given in the middle row set. In both experiments, we considered the output feature maps of base CNNs, and then applied global average pooling (GAP) prior to classification layer. In the last set of experiments (bottom row set), the erasing-based data augmentations remain the same.

Moreover, the attention module is applied as an alternative to GAP on base CNNs feature maps. However, the patches are not included in any baseline assessment (Fig. 4). The baseline performances have been improved using random erasing over traditional augmentation techniques. Also, attention has enhanced the baseline accuracy over GAP with a little overhead regarding the model parameters (approx +83K).

2) *SYD-Net’s Performance*: The accuracy of SYD-Net is improved significantly by incorporating an attention module (PbA) over hybrid patches. The performances of a different number of patches using four base CNNs *i.e.*, ResNet-50 (RN-50), DenseNet-201 (DN-201), MobileNet-v2 (MN-v2), and Xception (XN) are evaluated on all four datasets, and the results are given in Table IV. It evinces that uniform (U) patches could attain good results over baseline accuracy. Moreover, uniform patches in conjunction with hierarchical (H) regions boost the performance further by summarizing

TABLE IV

TOP-1 ACCURACY (%) OF SYD-NET (SCRATCH) WITH ATTENTION MODULES USING VARIOUS UNIFORM (U) AND HIERARCHICAL (H) PATCHES: P_9 , P_{12} , P_{16} , P_{20} , P_{25} , AND P_{30} . TWO RANDOM ERASED REGIONS WITH BASIC IMAGE AUGMENTATIONS ARE APPLIED.

| CNNs | Patch | Sports | Yoga82 | Yoga107 | Dance | Par(M) |
|--------|----------|--------------|--------------|--------------|--------------|--------|
| RN-50 | P_9 | 88.10 | 91.43 | 70.19 | 78.61 | 32.0 |
| | P_{12} | 89.37 | 92.56 | 70.67 | 79.03 | 32.7 |
| | P_{16} | 89.51 | 93.49 | 71.03 | 81.33 | 33.4 |
| | P_{20} | 90.23 | 93.77 | 71.90 | 82.52 | 34.2 |
| | P_{25} | 90.51 | 93.56 | 73.02 | 82.40 | 35.2 |
| | P_{30} | 91.37 | 93.92 | 75.00 | 84.18 | 36.2 |
| DN-201 | P_9 | 90.60 | 94.24 | 68.32 | 83.42 | 26.1 |
| | P_{12} | 91.32 | 94.94 | 69.71 | 83.00 | 26.8 |
| | P_{16} | 92.55 | 95.48 | 71.90 | 83.94 | 27.6 |
| | P_{20} | 92.85 | 95.75 | 72.32 | 85.24 | 28.3 |
| | P_{25} | 92.83 | 95.46 | 73.50 | 85.37 | 29.2 |
| | P_{30} | 93.36 | 95.87 | 74.73 | 88.03 | 30.0 |
| MN-v2 | P_9 | 93.50 | 94.66 | 75.26 | 84.36 | 7.5 |
| | P_{12} | 93.20 | 95.02 | 76.22 | 84.60 | 7.9 |
| | P_{16} | 92.90 | 95.06 | 77.67 | 85.42 | 8.4 |
| | P_{20} | 93.92 | 95.63 | 78.10 | 86.20 | 8.9 |
| | P_{25} | 93.22 | 94.96 | 78.84 | 86.85 | 9.6 |
| | P_{30} | 94.78 | 96.00 | 79.54 | 87.73 | 10.2 |
| XN | P_9 | 95.66 | 96.35 | 71.36 | 87.50 | 29.3 |
| | P_{12} | 95.89 | 96.68 | 77.72 | 89.21 | 29.9 |
| | P_{16} | 95.40 | 96.40 | 79.54 | 90.10 | 30.7 |
| | P_{20} | 96.03 | 96.76 | 80.19 | 90.22 | 31.5 |
| | P_{25} | 96.21 | 96.50 | 80.76 | 91.40 | 32.5 |
| | P_{30} | 96.70 | 97.29 | 82.00 | 92.24 | 33.5 |

TABLE V

SYD-NET'S TOP-1 ACCURACY(%) USING NASNETMOBILE (SCRATCH)

| Method | Sports | Yoga-82 | Yoga-107 | Dance | Param (M) |
|------------|--------|---------|----------|-------|-----------|
| Erasing BL | 70.82 | 77.61 | 56.20 | 66.35 | 4.4 |
| P_{20} | 90.62 | 94.08 | 72.70 | 83.88 | 9.8 |
| P_{30} | 91.58 | 94.70 | 74.09 | 84.12 | 12.4 |

contextual descriptions at multiple granularities. We have defined three sets of mixed patches: P_9 contains $3 \times 3 = 9$ (patch-size 16×16 pixels), P_{16} represents $4 \times 4 = 16$ (patch-size 12×12 pixels), and P_{25} represents $5 \times 5 = 25$ (patch-size: 9×9 pixels) uniform (U) regions. It is clear that more patches attain better results. For example, P_{25} renders better results than P_9 and P_{16} . To enhance the accuracy of uniform patches further, 3 hierarchical regions are included with P_9 to produce P_{12} (9U+3H) hybrid patches. Likewise, 4 multi-scale regions are included with P_{16} to generate P_{20} (16U+4H) patches, and 5 multi-scale regions are included with P_{25} to generate P_{30} (25U+5H) patches, respectively. The results imply that hybrid regions could improve accuracy over all three (P_9 , P_{16} , and P_{25}) sets of uniform patches. Finally, set P_{30} achieves the best performance among all patch sets. MobileNet-v2 achieves competitive results compared to heavier backbones. Thus, another light-weight CNN, NASNetMobile, is tested on these datasets additionally. Only the baseline with random erasing augmentation (Erasing BL), P_{20} , and P_{30} are considered in this precise experiment. The results of NASNetMobile trained from scratch are given in Table V. Both MobileNet-v2 and NASNetMobile, albeit lightweight, have attained competitive accuracy over other base CNNs.

Next, the top-5 accuracy (%) of SYD-Net using P_{30} with two random erased regions trained from scratch are given in Table VI. All backbone CNNs attain excellent top-5 accuracy on four SYD datasets. Now, SYD-Net is trained with pre-

TABLE VI

TOP-5 ACCURACY(%) OF SYD-NET WITH P_{30} , TRAINED FROM SCRATCH

| CNNs | Sports-102 | Yoga-82 | Yoga-107 | Dance-12 |
|--------------|------------|---------|----------|----------|
| ResNet-50 | 98.89 | 99.42 | 95.67 | 98.22 |
| DenseNet-201 | 99.40 | 99.20 | 96.20 | 98.93 |
| NASNetMobile | 99.07 | 99.60 | 95.99 | 98.69 |
| MobileNet-v2 | 99.60 | 99.78 | 97.95 | 98.70 |
| Xception | 99.81 | 99.42 | 98.39 | 99.70 |

trained *ImageNet* weights to observe its efficiency. This experiment is conducted with both lightweight CNNs, and the best performer Xception considering random erasing augmentation. The results are given in Table VII. The accuracy is improved by a significant margin using *ImageNet* weights on P_{20} and P_{30} compared to training from scratch (Table IV). Also, P_{30} offers a little accuracy gain over P_{20} .

Furthermore, SYD-Net is tested on the Yoga-107 dataset trained with *ImageNet* weight initialization using four base CNNs, considering all combinations of patches and random erasing data augmentation, as defined above. The top-1 accuracies are provided in Table VIII. The best performance on Yoga-107 is 87.17%, achieved by DenseNet-201 with P_{30} patches. Also, other CNNs have achieved competitive results, e.g., Xception achieved the second-best accuracy of 85.20%.

TABLE VII

TOP-1 ACCURACY (%) OF SYD-NET TRAINED WITH IMAGENET WEIGHTS USING TWO ERASED REGIONS WITH RANDOM VALUES

| CNNs | Model | Sports | Yoga-82 | Yoga-107 | Dance |
|--------------|----------|--------|---------|----------|-------|
| NASNetMobile | BL | 91.53 | 88.48 | 73.34 | 88.27 |
| | P_{20} | 97.56 | 94.44 | 83.92 | 95.80 |
| | P_{30} | 98.21 | 96.58 | 84.61 | 96.74 |
| MobileNet-v2 | BL | 93.11 | 90.73 | 75.64 | 87.38 |
| | P_{20} | 98.37 | 97.20 | 83.60 | 96.50 |
| | P_{30} | 98.70 | 97.41 | 85.14 | 96.80 |
| Xception | BL | 94.48 | 91.29 | 73.34 | 88.74 |
| | P_{20} | 98.81 | 97.41 | 84.18 | 97.15 |
| | P_{30} | 98.86 | 97.80 | 85.20 | 97.98 |

TABLE VIII

TOP-1 ACCURACY (%) OF SYD-NET TRAINED WITH IMAGENET WEIGHTS ON YOGA-107. THE TERMINOLOGIES ARE DENOTED AS: RN50 FOR RESNET-50; DN201 FOR DENSENET-201; XN FOR XCEPTION; MNV2 FOR MOBILENET-V2; BL FOR BASELINE; AND P_i FOR PATCHES.

| CNN | BL | P_9 | P_{12} | P_{16} | P_{20} | P_{25} | P_{30} |
|-------|-------|-------|----------|----------|----------|----------|--------------|
| RN50 | 74.20 | 80.76 | 81.99 | 82.42 | 83.11 | 83.60 | 85.04 |
| DN201 | 77.83 | 83.06 | 85.84 | 86.48 | 86.54 | 86.75 | 87.17 |
| MNV2 | 75.64 | 79.22 | 80.87 | 82.66 | 83.60 | 84.56 | 85.14 |
| XN | 74.41 | 82.21 | 83.65 | 83.97 | 84.18 | 84.33 | 85.20 |

3) *Model Parameters*: The complexity of SYD-Net in terms of model parameters estimated in millions (M) is given in the last column of Table III-V. MobileNet-v2 and NASNetMobile are lightweight backbones than other CNNs, regarding the model complexity. The model parameters of P_9 and P_{30} patch sets using MobileNet-v2 are 7.5M and 10.2M, respectively. Next, NASNetMobile's baseline parameters are 4.4M, and P_{30} requires 12.5M. Thus, the parametric complexity of P_{30} using NASNetMobile backbone is the second lowest (after 10.2M parameters of MobileNet-v2) among all five CNNs used here. MobileNet-v2 attains balanced performances on SYD datasets with lesser model parametric overhead,

whereas SYD-Net using Xception backbone has attained the best accuracy with higher model parameters (33.5M). The accuracies of other base CNNs are satisfactory, and useful for benchmarking the SYD datasets.

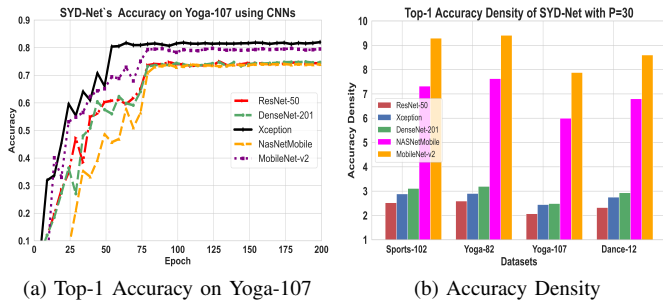


Fig. 10. Performance comparison of SYD-Net with P_{30} using five different backbone CNNs trained from scratch. (a) Top-1 accuracy on Yoga-107. (b) Accuracy density on four datasets using five backbone CNNs.

C. Comparative Study on Efficiency of Backbone CNNs

Few works tested on small-scale datasets have witnessed that MobileNet-v2 could achieve better performance than ResNet-50. A reason could be the fundamental design aspects of these standard backbones. ResNet family exploits shortcut connections (*i.e.*, identity mapping) to avoid performance degradation problem. This conjecture is further improved by introducing bottleneck layers where parameter-free identity shortcuts are crucial in the network at a deeper level. On the contrary, Xception is hypothesized by utilizing the inception module and separable convolutions for decoupling the spatial and channel-wise feature correlations. MobileNet-v2 is built upon the depth-wise and point-wise separable convolutions and the inverted residual with linear bottleneck layers. Moreover, ReLU6 non-linearity is used for handling robustness issues at a lower dimensional feature representation. Overall, this lightweight architecture directs to a faster and memory-efficient implementation than standard convolution, which is used as a main building block of other backbones. The compact, lightweight architecture of MobileNet-v2 leads to a higher computational and accuracy gain over other backbone CNNs. A comparative study on Yoga-107 using five base CNNs is shown in Fig. 10.a, and Xception renders the best accuracy among all CNNs. The results indicate superior performances of both lightweight CNNs compared to other heavier backbones, ResNet-50, and DenseNet-201 *i.e.*, densely connected between layers [64]. The results on Yoga-82, as reported in [8], imply that the MobileNet family outperforms the ResNet family. NASNetMobile attained competitive results *i.e.*, the differences between the accuracies of NASNetMobile and ResNet-50 on various fine-grained datasets are small in [20]. Thus, the results reported in various works evince the better capacity of lightweight MobileNet-v2 and NASNetMobile base CNNs. Herein, the efficacy of both lightweight CNNs is clear from the baselines and patched-based results.

To delve insight into the model's capacity, the performances of various base CNNs could be analyzed with the top-1 accuracy density, *i.e.*, the ratio of top-1 accuracy and the number of model parameters, as defined in [69]. A higher

accuracy density value implies a higher efficiency of a deep network. It indicates how efficiently the parameters contribute to the model's capacity and expressiveness through successive layers of transformation and non-linearity. In [69], MobileNet-v2 attained better accuracy density than other base CNNs, *e.g.*, ResNet-50. Our analysis of accuracy density follows a similar trend. A comparative study of accuracy density rendered by five base CNNs on four datasets is shown in Fig. 10.b. As aforesaid, a worthy reason of attaining a higher accuracy density is the powerful and precise architectural design of MobileNet-v2.

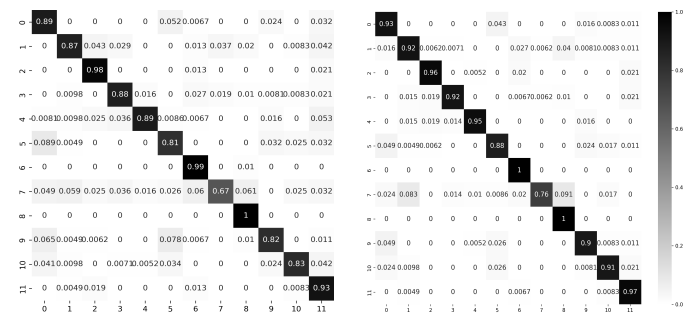


Fig. 11. Confusion matrices of SYD-Net with P_{30} on Dance-12 using MobileNet-v2, and Xception base CNNs. Best viewed in zoom.

D. Performance Comparison on Yoga-82 and Yoga-107

The pioneering work on Yoga-82, considering 82 classes and using a variant of DenseNet-201, has attained the best 79.35% top-1 and 93.47% top-5 accuracy, respectively. The performances on Yoga-82 using various CNNs are given in Table IX. The best performances of our approach are compared fairly using different CNNs trained from scratch. It is evident that SYD-Net outperforms those existing methods by a significant margin and achieves state-of-the-art results. The accuracies of our baseline methods are higher than actual Yoga-82. As a result, the top-1 and top-5 accuracy of SYD-Net using various CNNs are significantly higher than existing works on Yoga-82. The body key-points-based classifier ensemble method has achieved 80.14% top-1 accuracy [13]. Fusion of DenseNet-161 and KNN model achieves 79% accuracy while DenseNet-161 alone can attain 81% accuracy in Pose tutor [11]. On the contrary, SYD-Net has achieved at least a 14% gain in top-1 accuracy using various CNNs.

In Yoga-45 [7], 1931 images representing 45 yoga classes were selected and achieved 83.27% accuracy for pose grading using contrastive skeleton feature representation. In contrast, we have selected 5k images categorized into 107 classes as an enhanced version of Yoga-45. The best accuracy of SYD-Net is 87.17%, rendered by DenseNet-201 with ImageNet weight initialization, reported in Table VIII. However, our method is not directly comparable with Yoga-45 due to the differences in dataset characteristics (*e.g.*, sample size and the number of classes) and experimental setup.

The best top-1 accuracies of SYD-Net on four datasets using Xception, trained from scratch (srth), and ImageNet weights (ImNet) are reported in the last two columns of Table II. The proposed Sports-102 and Dance-12 datasets are publicly available for further improvement and comparative analysis.



Fig. 12. The tSNE plots of SYD-Net on Dance-12 using MobileNet-v2. Left to right: General baseline; Baseline with attention mechanism; SYD-Net with P_{25} , and finally, SYD-Net with P_{30} .

TABLE IX
COMPARISON OF TOP-1 AND TOP-5 ACCURACY(%) ON YOGA-82.

| Method | Backbone Types | Top-1 Acc | Top-5 Acc |
|----------------|----------------------|--------------|--------------|
| Yoga-82 [8] | MobileNet-V2 | 71.11 | 88.50 |
| | ResNet-50 | 63.44 | 82.55 |
| | DenseNet-201 variant | 79.35 | 93.47 |
| Ensemble [13] | keypoints + ensemble | 80.14 | - |
| Fusion [11] | DenseNet-161 (ImNet) | 81.00 | - |
| SYD-Net | ResNet-50 | 93.92 | 99.42 |
| | NASNetMobile | 94.70 | 99.60 |
| | DenseNet-201 | 95.87 | 99.20 |
| | MobileNet-v2 | 96.00 | 99.78 |
| | Xception | 97.29 | 99.42 |

E. Feature Maps Visualization

The confusion matrices of Dance-12 with P_{30} are shown in Fig. 11. We have delved into various key layers to visualize feature maps using the t-SNE [70] plots in Fig. 12. The figures show the feature distributions of data separability and clusters to reflect the discriminativeness of SYD-Net features. Here, the Dance-12 test set is considered for summarizing the feature distributions into a smaller subspace for visualization. In Fig. 12, the first two images show a comparison of feature representation between the traditional data augmentation and its improvement using the attention mechanism. Both techniques are considered as baselines. The last two t-SNE figures show feature representations of P_{25} and P_{30} in a lower dimension. These figures clearly show the class-wise feature map clusters with a significant class separability over the baselines. Also, the data distribution in P_{30} is slightly improved over P_{25} . This difference is reflected in the accuracy.

F. Ablation Study

The effectiveness of major components of SYD-Net is assessed on Dance-12 and Sports-102 using the MobileNet-v2 backbone. Mainly, the ablation study is focused on: (1) the patch-based attention module (PbA) and its sub-components; (2) the significance of two different activations in MLP; and (3) the impact of variations in random erasing data augmentations. The results are reported in Table X.

1) Patch-based attention module and its components:

We have evaluated the accuracy of three sets of hybrid patches without any attention module, i.e., P_{12} (9U+3H), P_{20} (16U+4H), and P_{30} (25U+5H) regions. The results imply that the inclusion of patches could improve the accuracy over the baseline performances, given in Table III. Also, P_{30} renders better accuracy compared to P_{12} and P_{20} .

The significance of channel attention and spatial attention mechanisms of SYD-Net are explored. We have tested both

TABLE X
ACCURACY (%) OF VARIOUS KEY COMPONENTS OF SYD-NET AND RANDOM ERASING AUGMENT USING MOBILENET-V2.

| SYD-Net components | Sports | Dance | Par |
|---|--------------|--------------|------|
| Using P_{12} only, no attention | 89.56 | 69.78 | 2.4 |
| Using P_{20} only, no attention | 86.94 | 68.54 | 2.4 |
| Using P_{30} only, no attention | 92.57 | 80.21 | 2.4 |
| Spatial attention only: SA_{12} | 77.18 | 67.71 | 3.9 |
| Spatial attention only: SA_{20} | 77.36 | 69.07 | 4.8 |
| Spatial attention only: SA_{30} | 78.54 | 69.55 | 6.1 |
| Channel attention only: CA_{12} | 91.44 | 74.88 | 6.4 |
| Channel attention only: CA_{20} | 91.53 | 76.12 | 6.4 |
| Channel attention only: CA_{30} | 94.00 | 77.54 | 6.4 |
| <i>sigmoid</i> spatial attention: SA_{12} | 77.62 | 70.31 | 3.9 |
| <i>sigmoid</i> spatial attention: SA_{20} | 93.06 | 84.89 | 8.9 |
| <i>sigmoid</i> spatial attention: SA_{30} | 93.90 | 85.96 | 10.2 |
| P_{12} with general dropout | 92.46 | 84.24 | 7.9 |
| P_{20} with general dropout | 93.85 | 84.83 | 8.9 |
| P_{30} with general dropout | 94.24 | 86.61 | 10.2 |
| P_{12} without <i>Gaussian</i> dropout | 93.06 | 83.29 | 7.9 |
| P_{20} without <i>Gaussian</i> dropout | 94.13 | 84.60 | 8.9 |
| P_{30} without <i>Gaussian</i> dropout | 94.82 | 85.60 | 10.2 |
| P_{30} with 1 erased region, rand RGB | 94.48 | 84.89 | 10.2 |
| P_{30} with 1 erased region, RGB=127 | 93.69 | 84.13 | 10.2 |
| P_{30} with 2 erased regions, RGB=127 | 94.52 | 86.43 | 10.2 |
| P_{30} , 2 erased regions, rand RGB: SYD-Net | 94.78 | 87.73 | 10.2 |

paths separately to analyze the effectiveness of attention mechanism in a performance gain. It is evident that the patch-based channel attention (CA) path is more beneficial than the spatial attention (SA) module. The reason could be that feature maps optimization across the channel dimension (MobileNet-v2: $7 \times 7 \times 1280$) is more effective over the spatial dimension ($7 \times 7 \times 2$). Because the feature space per patch is larger in cross-channel interaction than in spatial dimension, which ignores discriminative information during feature selection through spatial pooling. Also, P_{30} achieves better accuracy than P_{12} , as observed in earlier ablation studies.

2) Different activations in MLP and dropout layers: The effectiveness of *softmax* over *sigmoid* activation in the MLP layer of spatial attention is investigated. It is noted that *softmax* is more efficient in activating the neurons to estimate the probability maps for producing spatial attention masks. However, both activations are useful for improving overall accuracies leveraging the attention mechanism. The contribution of the *Gaussian* dropout (GD) is tested over the general dropout for regularization. It is evident that GD improves the learning task and enhances accuracy.

3) Variations in random erasing data augmentation: The performance of two randomly selected regions over a single region on input image during image augmentation is tested. The examples of random region erasing are illustrated in Fig. 3. The regions are non-overlapping, and the randomness of

related hyper-parameters (*e.g.*, size and color) of both regions are independent. SYD-Net is trained from scratch in two different erasing cases, *i.e.*, one with the random RGB values and another with a fixed RGB=127 value. In this test, we considered only P_{30} patches using MobileNet-v2. It implies that two erased regions could improve the accuracy compared to one erased region in both cases of RGB values. Because two smaller erased regions can learn more effectively than a larger erased region within the input image and improve the recognition accuracy. Also, random RGB performs slightly better than a fixed value RGB=127. The data augmentation of two erased regions with random RGB values performs more effectively in SYD-Net. Finally, the best model components of SYD-Net rendering the highest performance underlying MobileNet-v2 are given for completeness of ablation studies, implying the suitability of major components of the proposed SYD-Net architecture.

VI. CONCLUSION

This paper proposes a new patch-based attention method, called SYD-Net for fine-grained human posture recognition. We have introduced and benchmarked two new image datasets, representing 12-dance, and 102-sport actions with diversity. SYD-Net has achieved better performances on the Yoga-82 and Yoga-107 datasets. SYD-Net integrates fixed-size and multi-scale patches to learn contextual information and semantic understanding to define a comprehensive feature descriptor through spatial and channel attention. Random region erasing data augmentation also improves accuracy. Overall evaluation of various key components justifies the contribution of each module of SYD-Net. In the future, we plan to develop larger datasets on Sport and Dance styles and explore graph-based deep architecture for human posture recognition.

ACKNOWLEDGEMENT

The work and the contribution were also supported by the SPEV project, University of Hradec Kralove, Faculty of Informatics and Management, Czech Republic (ID: 2102–2023), “Smart Solutions in Ubiquitous Computing Environments”. We are also grateful for the support of student Michal Dobrovolny in consultations regarding application aspects. We thank to the Associate Editor and Reviewers for their comments to improve this paper. We thank to M. Verma [8], and repositories for providing their datasets used in this work. We are thankful to the BITS Pilani, Pilani Campus, Rajasthan, India, for providing the necessary infrastructure and Research Initiation Grant to carry out this work.

REFERENCES

- [1] G. Van Zandycke, V. Somers, M. Istasse, C. D. Don, and D. Zambrano, “Deepsporadar-v1: Computer vision dataset for sports understanding with high quality annotations,” in *Proc. 5th International ACM Workshop on Multimedia Content Analysis in Sports*, 2022, pp. 1–8.
- [2] S. Barbon Junior, A. Pinto, J. V. Barroso, F. G. Caetano, F. A. Moura, S. A. Cunha, and R. d. S. Torres, “Sport action mining: Dribbling recognition in soccer,” *Multimedia Tools and Applns.*, pp. 1–24, 2021.
- [3] J. Hwang, S. Park, and N. Kwak, “Athlete pose estimation by a global-local network,” in *Proc. IEEE Conf. on Computer Vision and Pattern Recognition Workshops*, 2017, pp. 58–65.
- [4] C. Dai, X. Liu, and J. Lai, “Human action recognition using two-stream attention based lstm networks,” *Applied Soft Computing*, vol. 86, p. 105820, 2020.
- [5] G. Thomas, R. Gade, T. B. Moeslund, P. Carr, and A. Hilton, “Computer vision for sports: Current applications and research topics,” *Computer Vision and Image Understanding*, vol. 159, pp. 3–18, 2017.
- [6] C. Zalluhoglu and N. Ikizler-Cinbis, “Collective sports: A multi-task dataset for collective activity recognition,” *Image and Vision Computing*, vol. 94, p. 103870, 2020.
- [7] Y. Wu, Q. Lin, M. Yang, J. Liu, J. Tian, D. Kapil, and L. Vanderbloemen, “A computer vision-based yoga pose grading approach using contrastive skeleton feature representations,” in *Healthcare*, vol. 10, no. 1. Multi-disciplinary Digital Publishing Institute, 2022, p. 36.
- [8] M. Verma, S. Kumawat, Y. Nakashima, and S. Raman, “Yoga-82: a new dataset for fine-grained classification of human poses,” in *Proc. IEEE/CVF Conference on Computer Vision and Pattern Recognition Workshops*, 2020, pp. 1038–1039.
- [9] S. K. Yadav, A. Agarwal, A. Kumar, K. Tiwari, H. M. Pandey, and S. A. Akbar, “Yognet: A two-stream network for realtime multiperson yoga action recognition and posture correction,” *Knowledge-Based Systems*, p. 109097, 2022.
- [10] J. Li, Q. Hu, T. Guo, S. Wang, and Y. Shen, “What and how well you exercised? an efficient analysis framework for fitness actions,” *Journal of Visual Comm. and Image Representation*, vol. 80, p. 103304, 2021.
- [11] B. Dittakavi, D. Bavikadi, S. V. Desai, S. Chakraborty, N. Reddy, V. N. Balasubramanian, B. Callepalli, and A. Sharma, “Pose tutor: An explainable system for pose correction in the wild,” in *Proc. IEEE/CVF Conf. Computer Vision and Pattern Recognition (CVPR)*, 2022, pp. 3540–3549.
- [12] S. K. Yadav, G. Singh, M. Verma, K. Tiwari, H. M. Pandey, S. A. Akbar, and P. Corcoran, “Yogatube: A video benchmark for yoga action recognition,” in *2022 International Joint Conference on Neural Networks (IJCNN)*. IEEE, 2022, pp. 1–8.
- [13] M. Chasmai, N. Das, A. Bhardwaj, and R. Garg, “A view independent classification framework for yoga postures,” *SN Computer Science*, vol. 3, no. 6, pp. 1–15, 2022.
- [14] J. Wang, Z. Wang, F. Gao, H. Zhao, S. Qiu, and J. Li, “Swimming stroke phase segmentation based on wearable motion capture technique,” *IEEE Trans. Instrum. and Measurement*, vol. 69, no. 10, pp. 8526–8538, 2020.
- [15] S. Samanta and B. Chanda, “Indian classical dance classification on manifold using jensen-bregman logdet divergence,” in *2014 22nd International Conf. Pattern Recognition (ICPR)*. IEEE, 2014, pp. 4507–4512.
- [16] P. Kishore, K. Kumar, E. Kiran Kumar, A. Sastry, M. Teja Kiran, D. Anil Kumar, and M. Prasad, “Indian classical dance action identification and classification with convolutional neural networks,” *Advances in Multimedia*, vol. 2018, 2018.
- [17] U. S. Tiwary *et al.*, “Classification of Indian classical dance forms,” in *International Conference on Intelligent Human Computer Interaction*. Springer, 2016, pp. 67–80.
- [18] A. D. Naik and M. Supriya, “Classification of Indian classical dance images using convolution neural network,” in *2020 Intl. Conf. Communication and Signal Processing (ICCSP)*. IEEE, 2020, pp. 1245–1249.
- [19] H. Bhuyan, P. P. Das, J. K. Dash, and J. Killi, “An automated method for identification of key frames in bharatanatyam dance videos,” *IEEE Access*, vol. 9, pp. 72 670–72 680, 2021.
- [20] A. Bera, Z. Wharton, Y. Liu, N. Bessis, and A. Behera, “Sr-gnn: Spatial relation-aware graph neural network for fine-grained image categorization,” *IEEE Transactions on Image Processing*, vol. 31, pp. 6017–6031, 2022.
- [21] Q. Wu, Y. Wu, Y. Zhang, and L. Zhang, “A local-global estimator based on large kernel cnn and transformer for human pose estimation and running pose measurement,” *IEEE Trans. Instrumentation and Measurement*, vol. 71, pp. 1–12, 2022.
- [22] Z. Wang, J. Li, J. Wang, H. Zhao, S. Qiu, N. Yang, and X. Shi, “Inertial sensor-based analysis of equestrian sports between beginner and professional riders under different horse gaits,” *IEEE Trans. Instrumentation and Measurement*, vol. 67, no. 11, pp. 2692–2704, 2018.
- [23] M. Habib, Z. Wang, S. Qiu, H. Zhao, and A. S. Murthy, “Machine learning based healthcare system for investigating the association between depression and quality of life,” *IEEE Journal of Biomedical and Health Informatics*, vol. 26, no. 5, pp. 2008–2019, 2022.
- [24] A. Mallik, S. Chaudhury, and H. Ghosh, “Nrityakosha: Preserving the intangible heritage of Indian classical dance,” *Journal on Computing and Cultural Heritage (JOCCH)*, vol. 4, no. 3, pp. 1–25, 2011.

- [25] S. Samanta, P. Purkait, and B. Chanda, "Indian classical dance classification by learning dance pose bases," in *2012 IEEE Workshop on the Applications of Computer Vision (WACV)*. IEEE, 2012, pp. 265–270.
- [26] A. Bisht, R. Bora, G. Saini, P. Shukla, and B. Raman, "Indian dance form recognition from videos," in *13th Int'l. Conf. Signal-Image Technology & Internet-Based Systems*. IEEE, 2017, pp. 123–128.
- [27] M. Skublewska-Paszowska, P. Powrozniak, J. Smolka, M. Milosz, E. Lukasik, D. Mukhamedova, and E. Milosz, "Methodology of 3d scanning of intangible cultural heritage—the example of lazgi dance," *Applied Sciences*, vol. 11, no. 23, p. 11568, 2021.
- [28] K. Kumar, P. Kishore, and D. Anil Kumar, "Indian classical dance classification with adaboost multiclass classifier on multifeature fusion," *Mathematical Problems in Engineering*, vol. 2017, 2017.
- [29] E. Hassan, S. Chaudhury, and M. Gopal, "Annotating dance posture images using multi kernel feature combination," in *2011 Third National Conf. Computer Vision, Pattern Recognition, Image Processing and Graphics*. IEEE, 2011, pp. 41–45.
- [30] S. Saha, S. Ghosh, A. Konar, and R. Janarthanan, "A study on leg posture recognition from Indian classical dance using kinect sensor," in *2013 Int'l. Conf. Human Computer Interactions*. IEEE, 2013, pp. 1–6.
- [31] A. P. Parameshwaran, H. P. Desai, M. Weeks, and R. Sunderraman, "Unravelling of convolutional neural networks through bharatanatyam mudra classification with limited data," in *10th Annual Computing and Communication Workshop and Conf*. IEEE, 2020, pp. 0342–0347.
- [32] S. Johnson and M. Everingham, "Clustered pose and nonlinear appearance models for human pose estimation," in *Proc. British Machine Vision Conf.* BMVA Press, 2010, pp. 12.1–12.11, doi:10.5244/C.24.12.
- [33] A. Vaswani, N. Shazeer, N. Parmar, J. Uszkoreit, L. Jones, A. N. Gomez, Ł. Kaiser, and I. Polosukhin, "Attention is all you need," *Advances in Neural Information Processing Systems*, vol. 30, 2017.
- [34] D. Bahdanau, K. Cho, and Y. Bengio, "Neural machine translation by jointly learning to align and translate," *arXiv preprint:1409.0473*, 2014.
- [35] M. Rey and A. Mnih, "Gaussian dropout as an information bottleneck layer," *Bayesian Deep Learning workshop*, 2021.
- [36] Z. Zhong, L. Zheng, G. Kang, S. Li, and Y. Yang, "Random erasing data augmentation," in *Proc. AAAI Conference on Artificial Intelligence*, vol. 34, no. 07, 2020, pp. 13 001–13 008.
- [37] T. Lan, Y. Wang, and G. Mori, "Discriminative figure-centric models for joint action localization and recognition," in *2011 International Conference on Computer Vision (ICCV)*. IEEE, 2011, pp. 2003–2010.
- [38] A. Karpathy, G. Toderici, S. Shetty, T. Leung, R. Sukthankar, and L. Fei-Fei, "Large-scale video classification with convolutional neural networks," in *Proc. IEEE Conf. Computer Vision and Pattern Recognition (CVPR)*, 2014, pp. 1725–1732.
- [39] T. K. K. Maddala, P. Kishore, K. K. Eepuri, and A. K. Dande, "Yoganet: 3-d yoga asana recognition using joint angular displacement maps with convnets," *IEEE Trans. Multimedia*, vol. 21, no. 10, pp. 2492–2503, 2019.
- [40] S. Samanta and B. Chanda, "A novel technique for space-time-interest point detection and description for dance video classification," in *International Symposium on Visual Computing*. Springer, 2013, pp. 507–516.
- [41] T. Han, H. Yao, C. Xu, X. Sun, Y. Zhang, and J. J. Corso, "Dancelets mining for video recommendation based on dance styles," *IEEE Transactions on Multimedia*, vol. 19, no. 4, pp. 712–724, 2016.
- [42] D. Castro, S. Hickson, P. Sangkloy, B. Mittal, S. Dai, J. Hays, and I. Essa, "Let's dance: Learning from online dance videos," *arXiv preprint arXiv:1801.07388*, 2018.
- [43] X. Hu and N. Ahuja, "Unsupervised 3d pose estimation for hierarchical dance video recognition," in *Proc. IEEE/CVF International Conference on Computer Vision (ICCV)*, 2021, pp. 11 015–11 024.
- [44] S. Shailesh and M. Judy, "Understanding dance semantics using spatio-temporal features coupled gru networks," *Entertainment Computing*, vol. 42, p. 100484, 2022.
- [45] S. Johnson and M. Everingham, "Learning effective human pose estimation from inaccurate annotation," in *Proc. IEEE/CVF Conf. Computer Vision and Pattern Recognition (CVPR)*. IEEE, 2011, pp. 1465–1472.
- [46] A. Mottaghi, M. Soryani, and H. Seifi, "Action recognition in freestyle wrestling using silhouette-skeleton features," *Engineering Science and Technology, an International Journal*, vol. 23, no. 4, pp. 921–930, 2020.
- [47] S. Liu, X. Liu, G. Huang, L. Feng, L. Hu, D. Jiang, A. Zhang, Y. Liu, and H. Qiao, "Fsd-10: a dataset for competitive sports content analysis," *arXiv preprint arXiv:2002.03312*, 2020.
- [48] P. Bharti, D. De, S. Chellappan, and S. K. Das, "Human: Complex activity recognition with multi-modal multi-positional body sensing," *IEEE Trans. Mobile Computing*, vol. 18, no. 4, pp. 857–870, 2018.
- [49] S. K. Yadav, A. Singh, A. Gupta, and J. L. Raheja, "Real-time yoga recognition using deep learning," *Neural Computing and Applications*, vol. 31, no. 12, pp. 9349–9361, 2019.
- [50] C.-H. Lin, S.-W. Shen, I. T. Anggraini, N. Funabiki, and C.-P. Fan, "An openpose-based exercise and performance learning assistant design for self-practice yoga," in *2021 IEEE 10th Global Conference on Consumer Electronics (GCCE)*. IEEE, 2021, pp. 456–457.
- [51] S. Bhambure, S. Lawande, R. Upasani, and J. Kundargi, "Yog-assist," in *2021 4th Biennial International Conference on Nascent Technologies in Engineering (ICNTE)*. IEEE, 2021, pp. 1–6.
- [52] C. Long, E. Jo, and Y. Nam, "Development of a yoga posture coaching system using an interactive display based on transfer learning," *The Journal of Supercomputing*, pp. 1–16, 2021.
- [53] I. Kapsouras, S. Karanikolos, N. Nikolaidis, and A. Tefas, "Feature comparison and feature fusion for traditional dances recognition," in *Intl. Conf. Engineering Applications of Neural Networks*. Springer, 2013, pp. 172–181.
- [54] S. Samanta and B. Chanda, "Space-time facet model for human activity classification," *IEEE Trans. Multimedia*, vol. 16, no. 6, pp. 1525–1535, 2014.
- [55] S. Dewan, S. Agarwal, and N. Singh, "Spatio-temporal laban features for dance style recognition," in *2018 24th International Conference on Pattern Recognition (ICPR)*. IEEE, 2018, pp. 2911–2916.
- [56] L. T. Bhavanam and G. N. Iyer, "On the classification of kathakali hand gestures using support vector machines and convolutional neural networks," in *2020 International Conference on Artificial Intelligence and Signal Processing (AISP)*. IEEE, 2020, pp. 1–6.
- [57] T. Mallick, P. P. Das, and A. K. Majumdar, "Posture and sequence recognition for bharatanatyam dance performances using machine learning approach," *arXiv preprint arXiv:1909.11023*, 2019.
- [58] V. Kaushik, P. Mukherjee, and B. Lall, "Nriyantar: Pose oblivious Indian classical dance sequence classification system," in *Proc. 11th Indian Conf. Computer Vision, Graphics and Image Processing*, 2018, pp. 1–7.
- [59] N. Jain, V. Bansal, D. Virmani, V. Gupta, L. Salas-Morera, and L. Garcia-Hernandez, "An enhanced deep convolutional neural network for classifying Indian classical dance forms," *Applied Sciences*, vol. 11, no. 14, p. 6253, 2021.
- [60] A. Bera, Z. Wharton, Y. Liu, N. Bessis, and A. Behera, "Attend and guide (ag-net): A keypoints-driven attention-based deep network for image recognition," *IEEE Transactions on Image Processing*, vol. 30, pp. 3691–3704, 2021.
- [61] M. Lin, Q. Chen, and S. Yan, "Network in network," *arXiv preprint:1312.4400*, 2013.
- [62] S. Woo, J. Park, J.-Y. Lee, and I. S. Kweon, "Cbam: Convolutional block attention module," in *Proc. European Conf. Computer Vision (ECCV)*, 2018, pp. 3–19.
- [63] K. He, X. Zhang, S. Ren, and J. Sun, "Deep residual learning for image recognition," in *Proc. IEEE Conf. Computer Vision and Pattern Recognition (CVPR)*, 2016, pp. 770–778.
- [64] G. Huang, Z. Liu, L. Van Der Maaten, and K. Q. Weinberger, "Densely connected convolutional networks," in *Proc. IEEE Conf. Computer Vision and Pattern Recognition (CVPR)*, 2017, pp. 4700–4708.
- [65] B. Zoph, V. Vasudevan, J. Shlens, and Q. V. Le, "Learning transferable architectures for scalable image recognition," in *Proc. IEEE Conf. Computer Vision and Pattern Recognition (CVPR)*, 2018, pp. 8697–8710.
- [66] M. Sandler, A. Howard, M. Zhu, A. Zhmoginov, and L.-C. Chen, "Mobilenetv2: Inverted residuals and linear bottlenecks," in *Proc. IEEE Conf. Computer Vision and Pattern Recognition (CVPR)*, 2018, pp. 4510–4520.
- [67] F. Chollet, "Xception: Deep learning with depthwise separable convolutions," in *Proc. IEEE Conf. Computer Vision and Pattern Recognition (CVPR)*, 2017, pp. 1251–1258.
- [68] K. He, X. Zhang, S. Ren, and J. Sun, "Spatial pyramid pooling in deep convolutional networks for visual recognition," *IEEE Trans. Pattern Analysis and Machine Intelligence*, vol. 37, no. 9, pp. 1904–1916, 2015.
- [69] S. Bianco, R. Cadene, L. Celona, and P. Napolitano, "Benchmark analysis of representative deep neural network architectures," *IEEE Access*, vol. 6, pp. 64 270–64 277, 2018.
- [70] L. Van der Maaten and G. Hinton, "Visualizing data using t-sne." *Journal of Machine Learning Research*, vol. 9, no. 11, 2008.